울산대학교 공학연구논문집 제33권 1호 pp. 129~144, 울산대학교.
Journal of Engineering Research Vol. 33, No. 1, pp. 129~144, 2002
University of Ulsan.

STATE ESTIMATION FOR AUTONOMOUS GUIDED VEHICLE USING THE EXTENDED KALMAN FILTER

Hansil Kim
Department of Electrical Engineering

This paper presents a four-wheel drive autonomous guided vehicle (AGV) system designed to transport unmanned control transportation (UCT) standard cargo containers in seaport environments. A model vehicle is simulated and experimented in laboratory and in a prepared road at speed up to 3 m/s. The navigation system is based on the use of encoder, gyro, and transponders at known locations in the environment. A general method for the construction of a positioning system is proposed, which is based on an extended Kalman filter (EKF) and commercially available navigation sensors in an absolute coordinate of AGV. The kinematics model and observation models are adapted for EKF application. Simulation result shows good performances of the AGV state estimator. *Copyright © 2002 IFAC*

Keywords: Extended kalman filter, autonomous guided vehicle, unmanned control transportation, state estimator, encoder, transponder

1. INTRODUCTION

This paper describes an Autonomous Guided Vehicle (AGV) system for transporting standard cargo containers in seaport environment and the design method for estimating the exact position using extended Kalman filter (EKF)[4,7]. There has been much interest in the development of AGV systems for a variety of applications[1,2] (Durrant-Whyte 1995, 1996; Thorpe et al. 1988). Much of the works was on the development of vehicles for rough terrain applications, using technology such as visual path image scanning[8], radar system, and global positioning system (GPS)[9] for positioning for control and guidance. The system presented in this paper utilizes different sensing and control units to estimate accurate absolute position. The vehicle is aimed specifically at a commercial-scale application that requires autonomous

navigation, and integration with supervisory system. In meeting these requirements, a cargo handling AGV must satisfy a number of functional requirements:

- Size: 3m x 0.6m (1/3 of actual size)
- Operation: Direct Drive DC motor with maximum speed 3m/s (Hydraulic actuator for real AGV normally with 6~8m/s)
- Environment: In the laboratory and on the well prepared road (to be adopted in all weather conditions for real AGV)
- Reliability: System failure must be minimized.
- Safety: The system must detect unexpected obstacles and avoid them.

In Section 2, the design of the overall vehicle is outlined, and the vehicle characteristics are exhibited as in the actual system. The kinematic model of AGV is represented and simplified to an equivalent 2-wheel steering system. These are subsequently used by the navigation and control systems for position estimation and trajectory tracking. In Section 3, the EKF related to the vehicle is described. The EKF exploits the model of the vehicle motion and its observations to continuously provide estimates of the vehicle location. This estimator of AGV system provides a solution to both position and accuracy requirements in a port environment. The estimator was tested for a 1/3 sized AGV model in a prepared road and laboratory with satisfactory performance, which gives good reference for the actual AGV design. Some of the difficulties in validating the design for outdoor AGV system are communications and networking constraints. In order to meet these conditions, we set the wireless networking protocol and sampling time at 10ms. The experiments performed in a commercial AGV and the results gained from the control and navigation systems are considered to be the most important contributions of this paper. The vehicle system described here was completed in December 2000 and has been in extensive trials at a container terminal in a seaport.

2. AGV SYSTEM MODELING

Fig. 1 shows a model AGV system for a container which is scaled down to 1/3 of the actual size presently used in sea port. The length between the front and rear axles is 3m and the width between the left and right wheels is 1.71m. All vehicle characteristics are exhibited as in the actual system. In this section, we construct the system model for observation utilizing incremental encoder, absolute encoder, fibre optic gyro, and transponder.

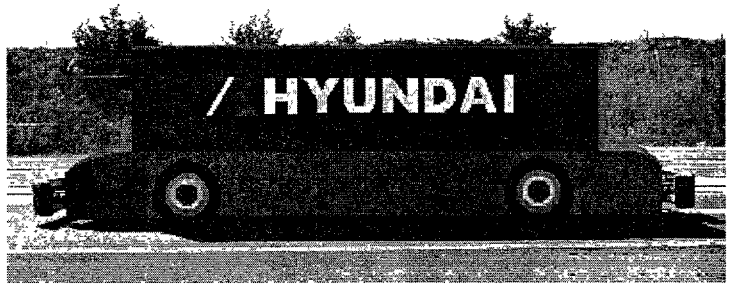

Fig. 1. Photograph of the 4-wheel steering AGV.

2.1 AGV Kinematics model

The AGV[6] consists of a 4-wheel steering drive in order to be able to turn even in a narrow space. The front wheel is independently linked to the rear wheel to turn and shift back and forth easily. We obtain the continuous state-space model for the 4 wheel steering system in this section. However, a 2-wheel steering system can be used to construct a simple dynamic model using steering angle and velocity of each wheel. To handle the 2-wheel steering AGV instead of the 4-wheel steering AGV, we simply placed an equivalent imaginary wheel replacing the left and right wheels for each axle. Fig. 2 shows a turning state of 4-wheel steered AGV, where L is the length between front and rear axles, w is the width of left and right wheel axes, TW is the gap between Kingpin and the center of wheel, ω is the velocity of each wheel, γ is the wheel angle, v is wheel velocity, ρ is a turning radius, and c is the distance from turning center to the central line of AGV.

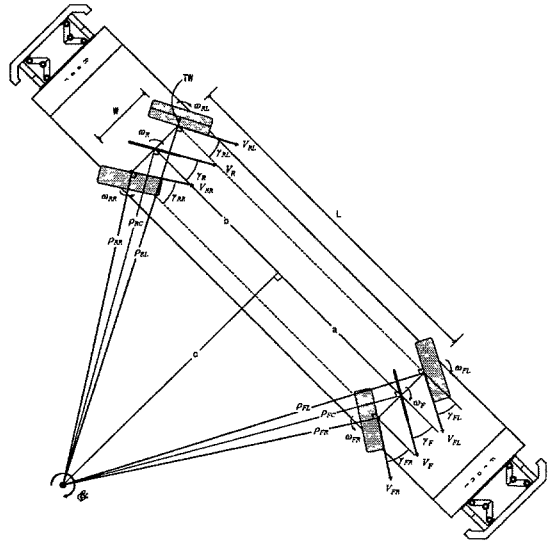

Fig. 2. Four-wheel steering AGV kinematic model.

The actual steering angle and wheel velocity can be determined by the turning radii. The imaginary steering angle of the front and rear wheels can be calculated by a steering angle of left and right wheels:

$$\gamma_F = \tan^{-1}\left(\frac{2\tan(\gamma_{FL})\cdot\tan(\gamma_{FR})}{\tan(\gamma_{FL})\cdot\tan(\gamma_{FR})}\right) \tag{1}$$

$$\gamma_R = \tan^{-1}\left(\frac{2\tan(\gamma_{RL})\cdot\tan(\gamma_{RR})}{\tan(\gamma_{RL})\cdot\tan(\gamma_{RR})}\right) \tag{2}$$

We will simply use γ_F and γ_R instead of γ_{FL}, γ_{FR}, γ_{RL} and γ_{RR} measured by encoder and gyro. The parameters a, b, and c are calculated in the following when AGV turns:

$$a = \frac{L\tan\gamma_F}{\tan\gamma_F+\tan\gamma_R},\ b = \frac{L\tan\gamma_R}{\tan\gamma_F+\tan\gamma_R},\ c = \frac{L}{\tan\gamma_F+\tan\gamma_R} \tag{3}$$

The turning radius of each wheel can be determined by

$$\rho_{FL} = \frac{a}{\sin\gamma_{FL}},\ \rho_{FC} = \frac{a}{\sin\gamma_{FC}},\ \rho_{FR} = \frac{a}{\sin\gamma_{FR}} \tag{4}$$

$$\rho_{FL} = \frac{b}{\sin\gamma_{FL}},\ \rho_{FC} = \frac{b}{\sin\gamma_{FC}},\ \rho_{FR} = \frac{b}{\sin\gamma_{FR}} \tag{5}$$

When the distance between Kingpin and center of wheel is not zero, the velocity v is not equal to the product of angular velocity of wheel and radius of wheel. As the angular velocity is the same as the turning velocity Φ of AGV, the velocity in Kingpin is calculated as follows:

$$V_{FL} = \frac{\rho_{FL}\cdot\omega_{FL}}{\rho_{FL}+TW}\cdot R,\ V_{FR} = \frac{\rho_{FR}\cdot\omega_{FR}}{\rho_{FR}-TW}\cdot R,$$
$$V_{RL} = \frac{\rho_{RL}\cdot\omega_{RL}}{\rho_{RL}+TW}\cdot R,\ V_{RR} = \frac{\rho_{RR}\cdot\omega_{RR}}{\rho_{RR}-TW}\cdot R \tag{6}$$

where ω is the angular velocity of each wheel and R is the radius of wheel.

The angular velocity of the imaginary wheel is given by the steering angle of left and right wheels and turning velocity:

$$\omega_F = 0.5 \times \frac{1}{\sin\gamma_F} \times \left(\frac{V_{FL}}{R} \cdot \sin\gamma_{FL} + \frac{V_{FR}}{R} \cdot \sin\gamma_{FR} \right)$$
$$\omega_R = 0.5 \times \frac{1}{\sin\gamma_R} \times \left(\frac{V_{RL}}{R} \cdot \sin\gamma_{RL} + \frac{V_{RR}}{R} \cdot \sin\gamma_{RR} \right) \quad (7)$$

The 4-wheel AGV kinematics model is simplified to a 2-wheel AGV kinematics model given in Fig. 3, where ${}^{A}X$ and ${}^{A}Y$ are Cartesian coordinates, and X and Y represent the center of AGV axis, and Φ is an angle between center line and the X axis.

The continuous state equation about center and gradient of AGV is expressed as follows:

$$\begin{aligned}
\dot{X}(t) &= \frac{1}{2} R(t)\{\omega_F(t)\cos(\Phi(t)+\gamma_F(t)) + \omega_R(t)\cos(\Phi(t)+\gamma_R(t))\} \\
\dot{Y}(t) &= \frac{1}{2} R(t)\{\omega_F(t)\sin(\Phi(t)+\gamma_F(t)) + \omega_R(t)\sin(\Phi(t)+\gamma_R(t))\} \\
\dot{\Phi}(t) &= \frac{1}{L} R(t)\{\omega_F(t)\sin(\gamma_F(t)) - \omega_R(t)\sin(\gamma_R(t))\} \\
\dot{R}(t) &= 0 \\
\ddot{\Phi}(t) &= \frac{1}{L} R(t)\{\dot{\omega_F}(t) \cdot \sin(\gamma_f(t)) + \omega_F(t) \cdot \cos(\gamma_F(t))\,\dot{\gamma_F}(t) \\
&\quad - \dot{\omega_R}(t) \cdot \sin(\gamma_R(t)) - \omega_R(t) \cdot \cos(\gamma_R(t))\,\dot{\gamma_R}(t)\}
\end{aligned} \quad (8)$$

where R(t) is the radius of wheel.

Equation (8) represents the dynamics of center, velocity, and acceleration of AGV. We add the acceleration part in (8) to compare the AGV state from Gyro sensor. Inputs to this model are the steering angle γ_F and γ_R, and the velocity of the wheels, ω_F and ω_R.

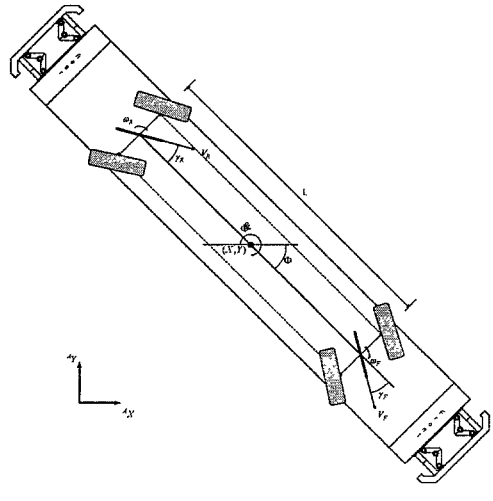

Fig. 3. Two wheel steering AGV Kinetic model.

We define $x_1(t)=X(t)$, $x_2(t)=y(t)$, $x_3(t)=\Phi(t)$, $x_4(t)=R(t)$, $x_5(t)=\dot{\Phi}(t)$ and the discrete-time state equation can be obtained as

$$\begin{aligned}
x_1(k+1) &= x_1(k)+dT\frac{x_4(k)}{2}\{\omega_F(k)\cos(x_3(k)+\gamma_F(k)) \\
&\quad +\omega_R(k)\cos(x_3(k)+\gamma_R(k))\} \\
x_2(k+1) &= x_2(k)+dT\frac{x_4(k)}{2}\{\omega_F(k)\sin(x_3(k)+\gamma_F(k)) \\
&\quad +\omega_R(k)\sin(x_3(k)+\gamma_R(k))\} \\
x_3(k+1) &= x_3(k)+dT\frac{x_4(k)}{L}\{\omega_F(k)\sin(\gamma_F(k)) \\
&\quad -\omega_R(k)\sin(\gamma_R(k))\} \\
x_4(k+1) &= x_4(k) \\
x_5(k+1) &= x_5(k)+dt\frac{x_4(k)}{L}\{domega_F(k)\cdot\sin(\gamma_F(k)) \\
&\quad -domega_R(k)\cdot\sin(\gamma_R(k)) \\
&\quad +\omega_F(k)\cdot\cos(\gamma_F(k))d\gamma_F(k) \\
&\quad -\omega_R(k)\cdot\cos(\gamma_R(k))d\gamma_R(k)\}
\end{aligned} \tag{9}$$

where dT is the sampling time of AGV system.

2.2 AGV observation model

The incremental encoder, absolute encoder, fiber optic gyro, and transponder sensors can be used to observe the state of AGV. We can obtain the moving velocity and angular velocity of AGV as

$$\begin{aligned}
V_X(k) &= \frac{R}{2}\{\omega_F(k)\cos(\Phi_G(k)+\gamma_F(k))+\omega_R(k)\cos(\Phi_G(k)+\gamma_R(k))\} \\
V_Y(k) &= \frac{R}{2}\{\omega_F(k)\sin(\Phi_G(k)+\gamma_F(k))+\omega_R(k)\sin(\Phi_G(k)+\gamma_R(k))\} \\
\Phi_G(k+1) &= \Phi_G(k)+dT\cdot\phi_G(k)
\end{aligned} \tag{10}$$

where G stands for Gyro.

Transponders are located on earth and the transponder sensor is mounted on AGV. Fig. 4 shows the transponder sensor measuring the signal from a transponder. If transponder sensor is mounted in parallel to the AGV axis, i.e., the implemented angle is zero, the position of transponder with respect to AGV is given by

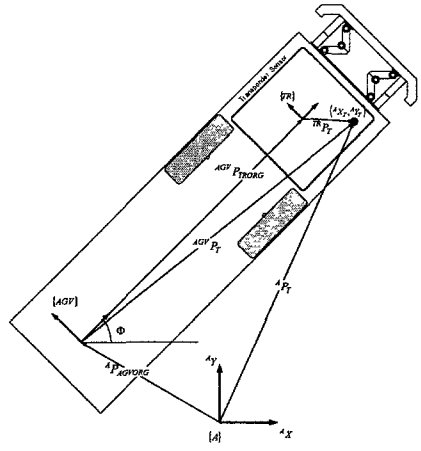

Fig 4. Mounting of transponder sensor

$$
\begin{aligned}
&{}^{A}P_T = {}^{A}P_{AGVORG} + {}^{A}_{AGV}R \cdot {}^{AGV}P_T \\
&{}^{A}_{AGV}R = \begin{bmatrix} \cos\Phi & -\sin\Phi \\ \sin\Phi & \cos\Phi \end{bmatrix} \\
&{}^{AGV}P_T = {}^{AGV}P_{TRORG} + {}^{AGV}_{TR}R \cdot {}^{TR}P_T \\
&{}^{AGV}_{TR}R = \begin{bmatrix} \cos\theta & -\sin\theta \\ \sin\theta & \cos\theta \end{bmatrix} = \begin{bmatrix} 1 & 0 \\ 0 & 1 \end{bmatrix} \\
&{}^{TR}P_T = {}^{A}_{AGV}R^T \cdot \left({}^{A}P_T - {}^{A}P_{AGVORG} \right) - {}^{AGV}P_{TRORG}
\end{aligned}
\tag{11}
$$

and the output measurement equation for transponder is given by

$$
\begin{bmatrix} {}^{TR}X_T(k) \\ {}^{TR}Y_T(k) \end{bmatrix} = \begin{bmatrix} \cos\Phi & \sin\Phi \\ -\sin\Phi & \cos\Phi \end{bmatrix} \cdot \begin{bmatrix} {}^{A}X_T(k) - {}^{A}X_{AGVORG}(k) \\ {}^{A}X_T(k) - {}^{A}Y_{AGVORG}(k) \end{bmatrix} - \begin{bmatrix} {}^{AGV}X_{TRORG} \\ {}^{AGV}Y_{TRORG} \end{bmatrix} \tag{12}
$$

where $({}^{A}X_T, {}^{A}Y_T)$ is the absolute position of transponder mounted on the earth, ${}^{AGV}P_{TRORG} = ({}^{AGV}X_{TRORG}, {}^{AGV}Y_{TRORG})$ is the position of transponder sensor with respect to the center of AGV, and ${}^{TR}P_T = \left({}^{TR}X_T(k), {}^{TR}Y_T(k) \right)$ is the position of transponder with respect to the transponder sensor.

3. DESIGN OF EKF

Kalman filter[5,7] is the optimal state estimator when white noises are implied to the system. It is a linear, unbiased, and minimum error variance recursive algorithm which

filters noises from the system when the signal is mixed with system noise and measurement noise. The extended Kalman filter (EFF) is a Kalman filter for a linearized system. As the AGV system is nonlinear, we need to linearize the AGV nonlinear model to apply the EKF. When this process is made, it is very important to preserve the characteristics of the nonlinear system. That means we should select the sampling time very carefully. The EKF can be used for estimating the turning angle of each wheel, angular velocity, and angular acceleration of AGV system.

We can summarize the EKF equation below. (Kwan and Lewis, 1999 and Kim and Sims, 1991):

Update state estimator:

$$\hat{x}^{+}(k) = \hat{x}^{-}(k) + W(k)[z(k) - \hat{z}(k)] \tag{13}$$

Predictor of the state equation:

$$\hat{x}^{-}(k+1) = f(\hat{x}^{+}(k)) \tag{14}$$

Measurement equation:

$$\hat{z}(k) = h(\hat{x}^{-}(k)) \tag{15}$$

Approximate system matrices:

$$\begin{aligned} F(k) &\cong \frac{\partial f(x(k), u(k))}{\partial x} \Big|_{x(k)=\hat{x}^{-}(k),\, u(k)=\hat{u}(k)} \\ G(k) &\cong \frac{\partial f(x(k), u(k))}{\partial u} \Big|_{x(k)=\hat{x}^{-}(k),\, u(k)=\hat{u}(k)} \\ H(k) &\cong \frac{\partial h(x(k), u(k))}{\partial x} \Big|_{x(k)=\hat{x}^{-}(k),\, u(k)=\hat{u}(k)} \end{aligned} \tag{16}$$

Kalman gain equation:

$$\begin{aligned} &P^{-}(k+1) = F(k)P^{+}(k)F^{T}(k) + G(k)\sum(k)G^{T}(k) \\ &P^{+}(k) = P^{-}(k) - W(k)S(k)W^{T}(k) \\ &W(k) = P^{-}(k)H^{T}(k)S^{-1}(k) \\ &S(k) = H(k)P^{-}(k)H^{T}(k) + \sum_{Z}(k) \end{aligned} \tag{17}$$

where $\sum(k)$and $\sum_{Z}(k)$ are the covariances of system noise and measurement

noise, respectively.

4. DESIGN OF STATE ESTIMATOR USING GYRO AND TRANSPONDER SENSORS

We can use both transponder sensor and gyro sensor when the transponders are placed on the ground. The initial condition for the EKF can be set by the previously estimated state when the AGV is in the next state with the measurement data. When only the gyro sensor is used, we need the information on the radius of wheel. But, when both sensors (transponder sensor and gyro sensor) are used, we dont need the information on the radius of wheel because the position can be measured.

The state variables are defined by

$$X_{GTS}(k)=[x_1(k)\ \ x_2(k)\ \ x_3(k)\ \ x_4(k)]^T=[X(k)\ \ Y(k)\ \ \Phi(k)\ \ \phi(k)]^T \tag{18}$$

The system matrix is given by

$$F(k)=\begin{bmatrix}1 & 0 & F_{13} & 0\\ 0 & 1 & F_{23} & 0\\ 0 & 0 & 1 & 0\\ 0 & 0 & 0 & 1\end{bmatrix}$$

$$F13=-dT\frac{R}{2}\{\ \overline{\omega}_F(k)\ s^+{}_{\phi\gamma F}(k)+\ \overline{\omega}_R(k)\ s^+{}_{\phi\gamma R}(k)\} \tag{19}$$

$$F23=-dT\frac{R}{2}\{\ \overline{\omega}_F(k)\ c^+{}_{\phi\gamma F}(k)+\ \overline{\omega}_R(k)\ c^+{}_{\phi\gamma R}(k)\}$$

where

$$\begin{aligned}
c^+_{\Phi_{\gamma F}}(k)&=\cos(\hat{x}^+_3(k)+\overline{\gamma}_F(k))\\
c^+_{\Phi_{\gamma R}}(k)&=\cos(\hat{x}^+_3(k)+\overline{\gamma}_R(k))\\
s^+_{\Phi_{\gamma F}}(k)&=\sin(\hat{x}^+_3(k)+\overline{\gamma}_F(k))\\
s^+_{\Phi_{\gamma R}}(k)&=\sin(\hat{x}^+_3(k)+\overline{\gamma}_R(k))
\end{aligned} \tag{20}$$

The observation matrix is given by

$$H(k)=\begin{bmatrix} -\cos(\hat{x}_3^-(k)) & -\sin(\hat{x}_3^-(k)) & H_{13} & 0 \\ \sin(\hat{x}_3^-(k)) & -\cos(\hat{x}_3^-(k)) & H_{23} & 0 \\ 0 & 0 & 0 & 1 \end{bmatrix}$$

$$\begin{aligned} H_{13} &= -({}^{A}X_T(k)-\hat{x}_1^-(k))\sin(\hat{x}_3^-(k)) \\ &\quad +({}^{A}Y_T(k)-\hat{x}_2^-(k))\cos(\hat{x}_3^-(k)) \\ H_{23} &= -({}^{A}X_T(k)-\hat{x}_1^-(k))\cos(\hat{x}_3^-(k)) \\ &\quad -({}^{A}Y_T(k)-\hat{x}_2^-(k))\sin(\hat{x}_3^-(k)) \end{aligned} \tag{21}$$

The output is given by

$$z(k)=\begin{bmatrix} {}^{TR}X_T(k) \\ {}^{TR}Y_T(k) \\ \phi_G(k) \end{bmatrix} \tag{22}$$

where the observations ${}^{TR}X_T(k)$ and ${}^{TR}Y_T(k)$ are expanded neighbourhood of ${}^{TR}\overline{X}_T(k)$ and ${}^{TR}\overline{Y}_T(k)$ with unknown disturbances $\delta X_{TS}$and $\delta Y_{TS}(k)$ respectively:

$$\begin{aligned} {}^{TR}X_T(k) &= {}^{TR}\overline{X}_T(k)(1+\delta\lambda_X(k))+\delta X_{TS}(k) \\ {}^{TR}Y_T(k) &= {}^{TR}\overline{Y}_T(k)(1+\delta\lambda_Y(k))+\delta Y_{TS}(k) \end{aligned} \tag{23}$$

The observation variance can be obtained by

$$\Sigma_{z_{GTR}}(k)=\begin{bmatrix} ({}^{TR}\overline{X}_T(k))^2\sigma_{\lambda_X}^2+\sigma_{X_{TS}}^2 & 0 & 0 \\ 0 & ({}^{TR}\overline{Y}_T(k))^2\sigma_{\lambda_Y}^2+\sigma_{Y_{TS}}^2 & 0 \\ 0 & 0 & \sigma_{\phi_G}^2 \end{bmatrix} \tag{24}$$

4. SIMULATION AND RESULTS

The performance of state estimation is different for different speed of AGV. We simulate the AGV for two different speed, 1m/s and 3m/s.

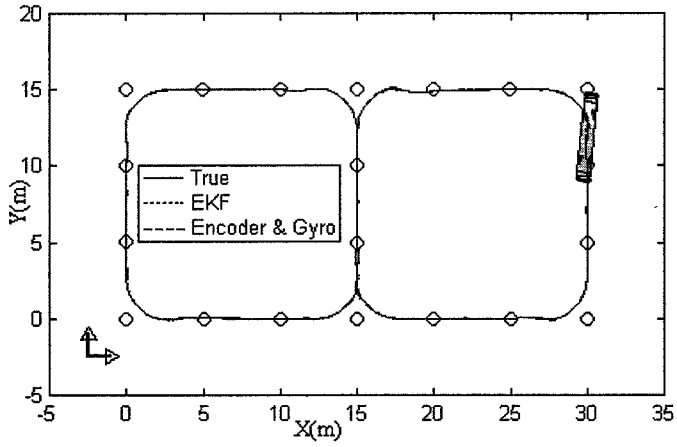

Fig. 5. The result of AGV running at 1m/s.

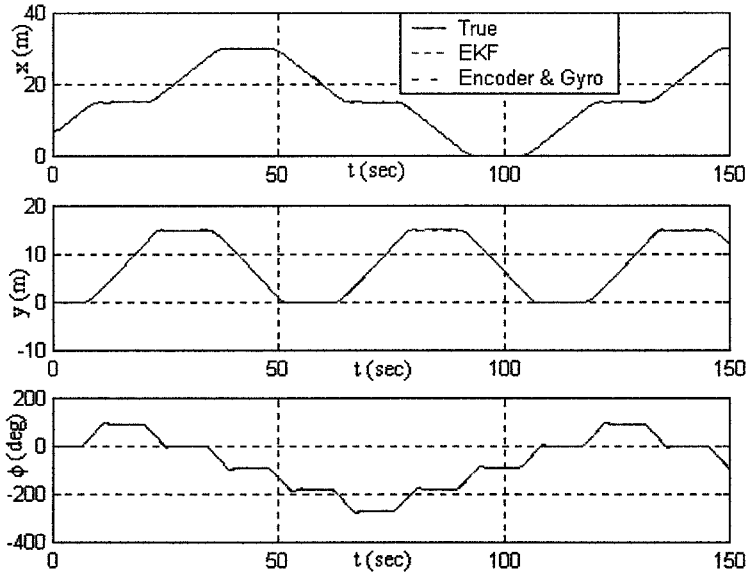

Fig. 6. The state changes of X, Y, and Φ.

Fig. 5 shows the path of AGV at the speed of 1m/s. We cannot differentiate the three plots from each other because all plots look the same. Fig. 6 magnifies certain area in Fig. 5. This gives us good estimation of the AGV current state. Fig. 7 shows changes of position (X,Y) and steering angles Φ.

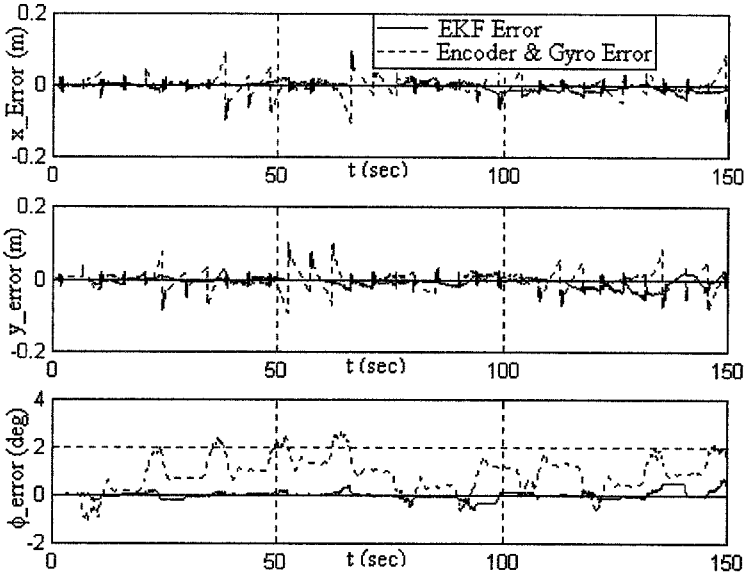

Fig. 7. The sate errors of X, Y, Φ.

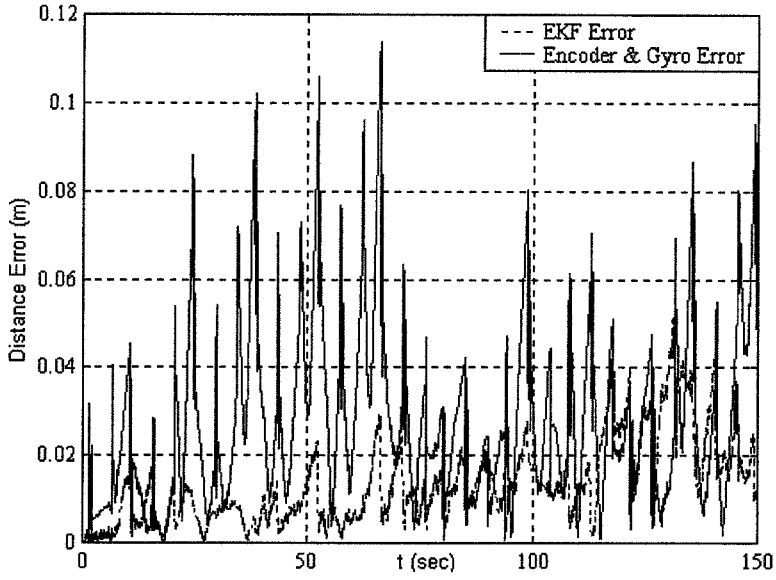

Fig. 8. The distance error of AGV.

The maximum change of the position is 5.88 cm. It is within the tolerance of our system (±30cm). Fig. 8 compares the distance error by the extended Kalman filter with the distance error from the encoder and Gyro measurements. Table 1 shows that the simulation result using EKF is more accurate than that only using encoder and gyro sensors.

Table 1. The result of maximum errors.

	X (Cm)	Y (Cm)	Φ(°)
Max. error of EKF	2.81	5.16	0.32
Max. error of E&G	9.77	17.86	1.47

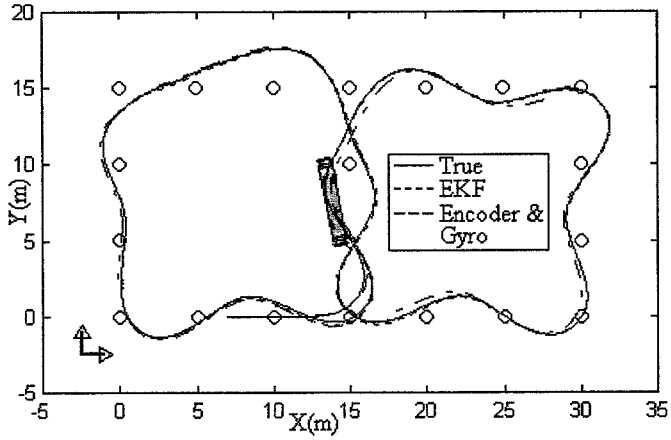

Fig. 9. The result of AGV running at 3 m/s.

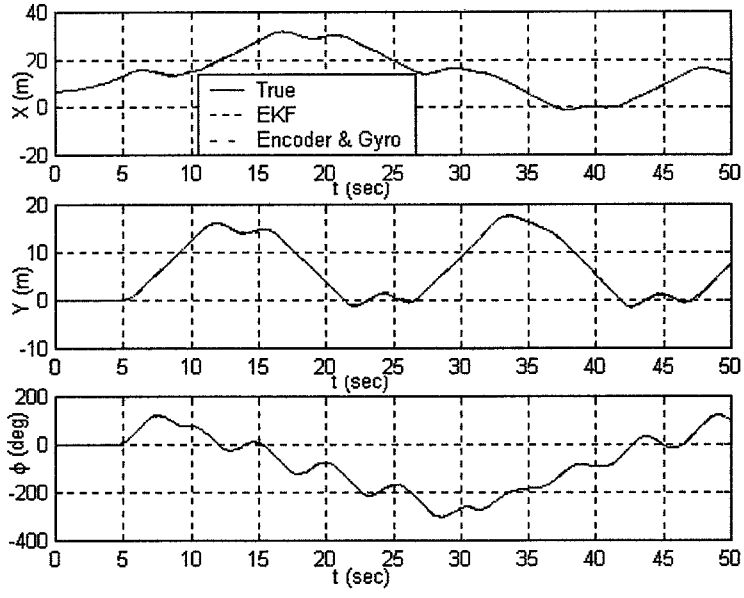

Fig. 10. The state changes of X, Y, Φ.

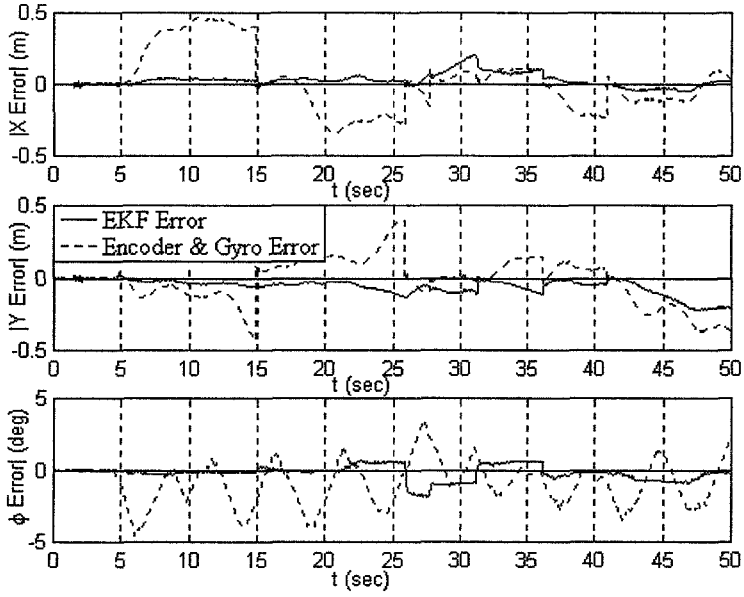

Fig. 11. The sate errors of X, Y, Φ.

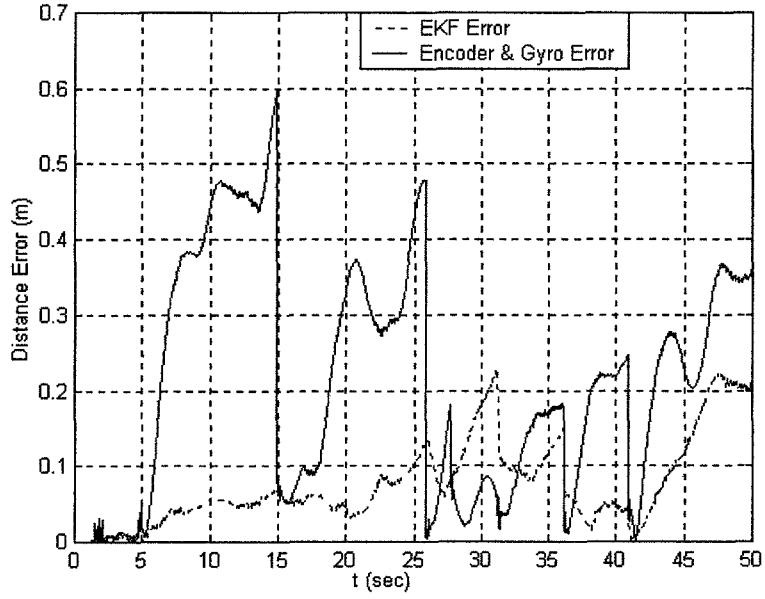

Fig. 12 The distance error of AGV.

Fig. 9 through Fig. 12 show the position and steering angle changes when the AGV runs at 3m/s. Fig. 9 shows the path of AGV at the speed of 3m/s. Figs. 10, 11, and 12 show the corresponding trajectories, position errors, and distance error, respectively. Table 2 summarizes the maximum errors and shows that the simulation result using

EKF is more accurate than that using only encoder and gyro sensors. The data from transponder and gyro sensors is effective within the region of ±30 cm from the center where a transponder is mounted. Otherwise, we can calculate the position using encoder and gyro sensors. The sampling time for the model AGV is required to be about 5.3ms in the extended Kalman filter (EKF) using a TMS320C32-50MHz DSP microprocessor. The overall delay is approximately 10 ms considering the time for calculation and communication with other network.

Table 2. Maximum error in estimation.

	X (Cm)	Y (Cm)	Φ(°)
Max. error of EKF	5.13	11.96	0.44
Max. error of E&G	48.59	65.35	3.62

Examining the result when the AGV navigates at 3 m/s, it is noted that the AGV cannot estimate the true trajectory when we use encoder and gyro sensor only. We need the extended Kalman filter to meet the tolerance condition. When the AGV cannot recognize transponder or turns a corner, it uses only encoder and gyro sensor in dead reckoning intervals. The position errors are increased somewhat. But, since the moving distance is not too long, it will not be a problem to track the desired route.

5. CONCLUSION

The state estimator is designed for AGV using the incremental encoder, absolute encoder, fiber optic gyro sensor, and transponder. The position estimation with transponder and gyro sensors is more accurate than the direct measurement with encoder and gyro sensors. In the simulation, a satisfactory performance has been achieved, where the error range is within the tolerance (±30 cm) with respect to exact position. Although the experimental results are not shown here, the 1/3-sized AGV was tested in a prepared road and in laboratory with good performance. This design will be applied to a real size AGV to navigate in a seaport in future.

REFERENCES

1. De, Wit C. C. and Tsiotras P. (1999). Dynamic Tire Friction Models for Vehicle Traction Control. In: *Proc. the 38th IEEE Conference on Decision and Control*, **vol. 4**, pp. 3746 3751.
2. Durrant-Whyte, H. F. (1995). The Design of a Radar-Based Navigation System for

Large Outdoor Vehicles. In: *Proc. IEEE International Conference on Robotics and Automation*, **vol. 1**, pp. 764 769.

3. Durrant-Whyte, H. F. (1996). An Autonomous Guided Vehicle for Cargo Handling Applications. *The international Journal of Robotics Research*, **vol. 15, no. 5**, pp. 407 440.
4. Jetto, L., S. Longhi, and G. Venturini (1999). Development and Experimental Validation of an Adaptive Extended Kalman Filter for the Localization of Mobile Robots. In: *IEEE Transactions on Robotics and Automation*, **vol 15, no 5**, pp. 219-229.
5. Kim, H. and C. S. Sims (1991). Observer Based Stochastic Filtering and Control In: *Proc. American Control Conference*, Boston, MA, pp. 2839-2840.
6. Kluge, K. and C. Thorpe (1989). Explicit models for robot road following. In: *IEEE Conference on Robotics and Automation*, **vol. 2**, pp. 1148-1154.
7. Kwan, C. M and Lewis, F.L (1999). A Note on Kalman Filtering. In: *IEEE Transactions on Robotics and Automation*, **vol. 42, no 3**, pp. 225 227.
8. Thorpe, C., M.H Hebert, T. Kanade, and S.A. Shafer (1988). Vision and navigation for the Carnegie-Mellon Navlab. In: *IEEE Transactions on Pattern Analysis and Machine Intelligence*, **vol. 10, issue 3**, pp. 362373.
9. Wada, M., S. Kang and H. Hashimoto (2000). High accuracy road vehicle state estimation using extended Kalman filter In: Proc. *IEEE Intelligent Transportation Systems*, pp. 282 287.